JOURNAL OF PROPULSION AND POWER
Vol. 22, No. 4, July–August 2006

# High-Frequency Transverse Acoustic Coupling in a Multiple-Injector Cryogenic Combustor

Franck Richecoeur,* Philippe Scouflaire,† Sébastien Ducruix,‡ and Sébastien Candel§
*Ecole Centrale Paris, 92295 Châtenay-Malabry, France*

**High-frequency combustion oscillations are investigated experimentally. The combustor fed by cryogenic propellants operates under elevated pressure conditions ($p_c = 0.9$ MPa) and is equipped with three coaxial injectors fed by liquid oxygen and gaseous methane. Injection parameters are in the typical range used in rocket engines. This experiment simulates on a model scale conditions prevailing in such systems, but full similarity is not achieved. The chamber exhibits a set of resonant modes with eigenfrequencies above 1 kHz. The study focuses on high-frequency dynamics resulting from a strong coupling between one of the transverse modes and combustion. The combustor is forced with an external actuator. The eigenmodes are identified with a linear frequency sweep, and then the system is modulated at the first transverse resonant frequency. The flame motion and response are observed with a high speed and two intensified charge-coupled-device cameras recording phase-conditioned images. In a set of experiments carried out on the multiple-injector combustor, operating conditions were changed systematically to determine parameter ranges leading to combustion sensitivity to transverse excitation. Strong coupling is observed in this way with a spectacular modification of the flame spread. Emission from the three flames is notably intensified when this coupling occurs, whereas thermocouples placed on the lateral walls detect a rapid increase in temperature. The OH* emission intensity that can be linked to the heat-release rate is increased. A phase analysis indicates that the pressure and OH* emission oscillate transversally and in phase at the modulation frequency. This behavior is also observed with the high-speed camera, which also features enhanced reactive vortices convected in the downstream direction at a lower frequency.**

## I. Introduction

MUCH research in combustion has focused on instability mechanisms.[1] Investigations have concerned fundamental instabilities of flames and combustion dynamics phenomena encountered in practical devices. Recent work has focused on gas turbines of the premixed type with an emphasis on low-frequency oscillations coupled by plane acoustic modes of the system.[2] Model-scale experiments have provided a large amount of data leading to a general understanding of the fundamental processes.[3,4] Large-eddy simulations have been developed in parallel to represent dynamical combustion effects and devise predictive tools. Less experimental work has been carried out on high-frequency (HF) oscillations. Such HF instabilities are most often observed in rocket engines, where they are coupled by transverse chamber modes,[5] but they also appear in annular gas-turbine combustors. Most of the data in this frequency range were generated during the early development of rocketry when instability problems were continuously encountered and hampered many projects inducing serious problems and some spectacular failures.[6,7] Laboratory-scale experiments were carried out during the late 1960s and early 1970s,[8–10] but a detailed characterization of the driving and coupling phenomena was not completed because of limitations in experimentation, diagnostics, and digital data-processing hardware.

Little progress has been made in this field since that time because of a lack of fundamental information. It was therefore timely to take a new look at the problem, design a well-controlled model-scale experiment, and use state-of-the-art diagnostic tools. Some recent small-scale experiments have provided useful data on the injection process of cryogenic propellants under an external acoustic modulation.[11,12] These experiments featured a strong effect of the transverse acoustic wave on the atomization process. The liquid jet expansion rate increases significantly. However, these cold-flow tests only partially reproduce hot-fire conditions, and effects on heat release cannot be extracted from these measurements. The dynamics of injectors are also relevant, and these are well discussed in Ref. 13 but again under cold-flow conditions. The experimental effort is also accompanied by new simulations of the acoustic behavior of combustion chambers.[14,15] From this review it appears that effects of transverse acoustic modulations on multiple cryogenic flames have not been examined up to now. Much of the research work has concerned longitudinal perturbations, and most of the recent experiments involve premixed combustors designed for low NOx gas turbines and aeroengines. These are clearly not too relevant to rocket engines.

It is sometimes felt that is not possible to study high-frequency instabilities outside real systems because conditions prevailing in these devices cannot be reproduced in model-scale experiments. This mismatch between real and laboratory-scale systems has been one important difficulty of experimental research, and it is only partially overcome in the present study. One can however envisage to study some of the fundamental processes by suitably designing the experiment and properly choosing operating conditions and injection parameters.[16,17] It is not possible to reproduce all of the complexity of rocket engines, but some of the essential aspects are conserved.[18]

To this purpose, the model-scale combustion chamber is fed with real cryogenic propellants, it operates at an elevated pressure, and injection conditions are in the range characterizing real engines. The chamber is equipped with shear coaxial injectors similar to those used in current engines.[19] The combustor geometry features well-separated resonant modes[20] and characteristic eigenfrequencies in the standard range where high-frequency instabilities usually occur ($f > 1$ kHz).[21,22] The present experimental design relies heavily on recent knowledge gathered on the processes of cryogenic propellant combustion.[23] Operating conditions are deduced

Received 1 July 2005; revision received 13 January 2006; accepted for publication 16 January 2006. 

*Ph.D. Student, Laboratoire EM2C, Centre National de la Recherche Scientifique.
†Research Engineer, Laboratoire EM2C, Centre National de la Recherche Scientifique.
‡Research Scientist, Laboratoire EM2C, Centre National de la Recherche Scientifique.
§Professor, ECP and IUF, Laboratoire EM2C, Centre National de la Recherche Scientifique. Fellow AIAA.

from those determined in these studies. The momentum flux ratio between gaseous methane and liquid oxygen is in the range corresponding to real operation. The flame lengths are typical of those found in practice ($l_f/d_{\mathrm{LOx}} \simeq 50$).

One idea explored in the present work is that collective interactions involving neighboring flames constitute a fundamental source of combustion instability. This is supported by recent experiments on premixed flames, which indicate that strong sources of instability are most often related to interactions.[24,25] It has been shown for example that flames interacting with walls can become a powerful source of instability. Other experiments on flame/flame interactions indicate that colliding flame layers can be a strong source of self-induced oscillations. One particular characteristic of rocket engines is their showerhead arrangement of reactant jets. The closely packed flame geometry produces interactions in the vicinity of the chamber backplane. Collisions between adjacent streams can enhance turbulence and augment the volumetric rate of reaction. There is a natural delay in this process and a possibility of tuning the collision process with one of the acoustic resonances.[26] This is why one should examine collective effects involving more than a single jet.

These fundamental effects have not been extensively investigated in the past, or at least no conclusions were drawn on the possible collective effects of such arrangements of highly reactive jets. Previous experiments with liquid oxygen and gaseous hydrogen have been carried out on the test bench.[20] These gave relevant information on the combustion process and the feasibility of the experiment, but the low level of pressure fluctuations did not allow the description of the possible role of collective effects.

This paper begins with a brief description of the experimental configuration and diagnostics. External modulation is used to induce the transverse motion. The efficiency of the modulation system is an important parameter in the present investigation. This factor has been improved by various changes in the modulator design, which are explained in a separate section. Experimental results presented next indicate that under certain conditions the coupling between external modulation and combustion can be quite powerful.

## II. Experimental Configuration and Diagnostics

### A. Multiple-Injector Test Bench

The experimental setup involves three main elements: a combustion chamber and a cryogenic feed system, three coaxial injectors forming jet flames inside the chamber, and an external source of modulation to excite one of the chamber transverse modes. The chamber has a rectangular cross section with dimensions equal to $350 \times 250 \times 50$ mm$^3$. The combustor dimensions have been chosen to place the eigenfrequencies in the frequency range of instabilities in real engines (above 1 kHz). Its small spanwise thickness ($l_z = 50$ mm) is such that the pressure perturbations in the transverse direction can only occur at very high frequencies. It is designed to sustain a chamber pressure up to 7 MPa, and it is thus possible to exceed the critical pressure of oxygen (i.e., $p_{\mathrm{cr}} = 5.04$ MPa). In the present hot-fire tests the maximum nominal pressure is 0.9 MPa. The upper and lower walls of the chamber are respectively equipped with three and two pressure transducers (namely, C1 to C5 in Fig. 1) while the lateral side walls comprise large transparent quartz windows ($150 \times 100$ mm$^2$) allowing direct observation of the three flames in the visible and near UV ranges.

The coaxial injectors are similar to those used in practice, with external methane diameter $d_{\mathrm{CH_4}} = 1.25 d_{\mathrm{LOx}}$ and a distance between the injectors of $3.4 d_{\mathrm{LOx}}$, which is significantly larger than that of real engines. Methane is injected at ambient temperature, or it is cooled down to 180 K while the oxygen temperature is maintained at 80 K. The momentum flux ratio $J$ ($= \rho_{\mathrm{CH_4}} U_{\mathrm{CH_4}}^2 / \rho_{\mathrm{LOx}} U_{\mathrm{LOx}}^2$) between the gas and liquid streams is chosen in a range that is typical of real systems. The total oxygen flow rate is 60 g s$^{-1}$, corresponding to $U_{\mathrm{LOx}} = 2.8$ m s$^{-1}$, while the methane flow rate is varied from 50 to 100 g s$^{-1}$, giving rise to mean flow velocities $U_{\mathrm{CH_4}} = 90$ to 180 m $\cdot$ s$^{-1}$. With these parameters, the flame spreads over $25 d_{\mathrm{LOx}}$ to $45 d_{\mathrm{LOx}}$ depending on the methane injection velocity.

Velocities outside the jets are admittedly lower than those found in engines because the available cross section is larger. However, the flame is located between the inner oxygen stream and the coannular methane jet, and it is only weakly influenced by the outer flow. The chamber volume is relatively large to obtain a transverse mode in the proper frequency range. The volumetric heat release $(\dot{m}_{\mathrm{LOx}} \Delta h)/V = 0.06 \times 1.25\ 10^7 / 4.375\ 10^{-3} \simeq 170$ MW m$^{-3}$ is relatively low when compared to that characterizing a real engine (10 to 50 GW m$^{-3}$). This could be increased by augmenting the number of injectors and the mass flow rate of oxygen. One would also like to decrease the injector spacing to pack the injectors more closely and reduce the interaction distance, but mechanical constraints could not be overruled.

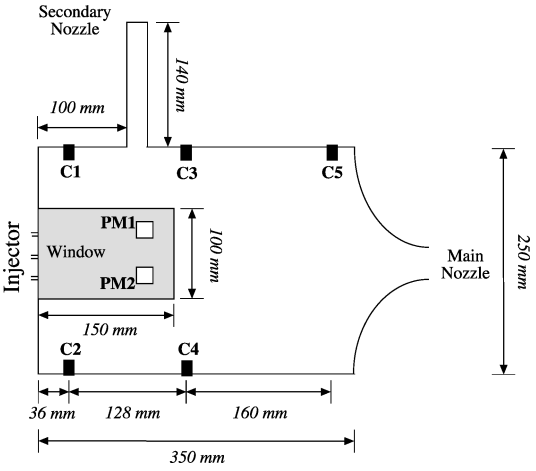


**Fig. 1 Schematic of the multi-injector combustion chamber.**

The test combustor is naturally stable. There is no dominant frequency in the pressure signals recorded without external modulation. The power spectral density of the signals reveals peaks for the chamber eigenfrequencies only when the data are high-pass filtered with a cutoff frequency of 1 kHz. To perturb the system, the modulation has to be generated externally to induce a coupled combustion oscillation. Linear transverse modulation is envisaged, and the system has to be permanently excited because self-sustained oscillations are not observed. A secondary nozzle, placed 100 mm from the chamber backplane on the top wall, is used to eject up to 15% of the total flow rate under steady conditions. The nozzle is periodically blocked by a rotating toothed wheel with a diameter of 185 mm comprising 50 5-mm large teeth regularly distributed around its external border. The real flow rate ejected through the modulation nozzle is less than 7.5% because of the periodic obstruction. With this secondary nozzle, part of the gases are periodically evacuated from the combustor in the cross-stream direction. Because of this ejection, the auxiliary nozzle acts as a pressure source, which generates transverse pressure waves in the chamber. The various eigenmodes of the system can be excited by changing the modulation frequency (i.e., the rotation speed of the toothed wheel). This apparatus effectively generates strong well-controlled acoustic oscillations in the chamber.[20]

### B. Diagnostics

A set of diagnostics is used under hot-fire tests to characterize the acoustic behavior of the chamber and observe the combustion process and the direct effect of the modulation on the flame sheets. Figure 2 shows the experimental setup.

Five Kistler pressure sensors (type 701A) are placed in the chamber walls (three in the top walls and two in the bottom ones). Their signals are sampled at a 40-kHz rate. Each pressure sensor has a resonant frequency of 70 kHz, which is significantly higher than the frequency range of interest. The relative position of the sensors is such that the phase between each of these probes can be used to describe the acoustic mode generated in the chamber. Two additional pressure transducers are located on the LOx and $CH_4$ injection lines but at a distance from the injector inlet sections. These transducers cannot be placed closer to these units because of the complicated configuration of the injection plane. Their signals are therefore less easy to interpret and will not be analyzed in what follows.

Combustion is observed with two intensified cameras providing flame images at 20 frames per second. Light emission from OH$^*$

**Table 1 Operating points tested during the hot-fire test series**

| Points | $\dot{m}_{CH_4}$, $g \cdot s^{-1}$ | $U_{CH_4}$, $m \cdot s^{-1}$ | $T_{CH_4}$, K | $\dot{m}_{LOx}$, $g \cdot s^{-1}$ | $U_{LOx}$, $m \cdot s^{-1}$ | $T_{LOx}$, K | $E$ | $J$ |
|---|---|---|---|---|---|---|---|---|
| F50-T280 | 50 | 90 | 280 | 60 | 2.8 | 80 | 1.2 | 5.4 |
| F70-T280 | 70 | 115 | 280 | 60 | 2.8 | 80 | 0.85 | 12 |
| F100-T280 | 100 | 150 | 280 | 60 | 2.8 | 80 | 0.6 | 20 |
| F50-T180 | 50 | 65 | 180 | 60 | 2.8 | 80 | 1.2 | 4.6 |

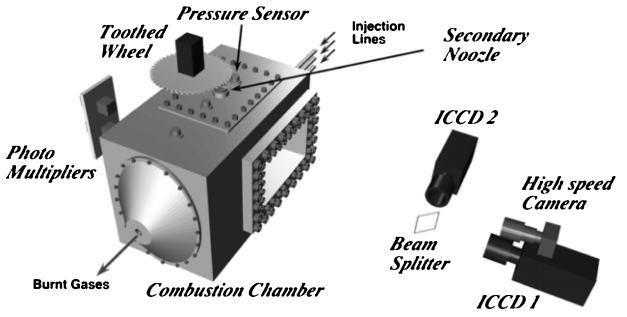


**Fig. 2 Multiple-injector combustor and diagnostics.**

radicals is used to track the flame position. The use of gaseous methane allows also to observe emission from $CH^*$ radicals. Images obtained by recording light emitted in $OH^*$ and $CH^*$ bands show similar spatial distributions of intensity. It was decided to use $OH^*$, which provides a better signal-to-noise ratio. The levels of intensity of these radicals give also precious information about the combustion intensity. Narrowband filters are used to observe the light emission from $CH^*$ and $OH^*$ radicals. $OH^*$ is observed by combining UG-11 and WG-305 filters creating a range of interest between 300 and 340 nm, while GG400 and SWP 604 filters are used to observe $CH^*$ radicals emission.

The exposure time is chosen to freeze the flow during each frame. High-speed imaging of the combustion process shows that the reactive structures are convected at a velocity close to 50 $m\ s^{-1}$, which corresponds to half the sum of the gaseous- and liquid-phase initial velocities. An exposure time equal to 6 $\mu$s corresponds to a typical displacement of 0.3 mm, which is the size of one pixel in our setup.

A high-speed camera operating at 20,000 frames per second provides information on the flame dynamics and interactions. At this frequency, the whole window area cannot be seen, and a region of interest is chosen where the collective interactions between the three flames occur. This window is located at a distance of 12 cm from the injection plane. The camera collects the visible emission originating from the flames.

A thermocouple measures the temperature at the lower chamber wall. The thermocouple response is limited to 10 Hz, and this probe does not provide high-frequency data about the wall temperature but yields useful information on the mean evolution of the wall temperature.

Finally, two photomultipliers (PM) describe the instantaneous combustion intensity in the chamber. These sensors are located at an axial distance of 11 cm from the injection plane and are vertically aligned. Spatial filters are used to focus the upper PM on the top part of the chamber while the lower PM is focused on the bottom part of the chamber. This setup can be used to examine the phase relations between upper and lower light emission regions.

### C. Operating Points

Previous experiments were carried out with liquid oxygen and gaseous hydrogen,[20] but the resulting flames were stable, and the modulation system generated insufficient levels of pressure oscillations. Modifications of the flames were observed, but the amplitude was too low to detect a profound change in the flame expansion rate and dynamics.

The present hot-fire tests were carried out with gaseous methane and liquid oxygen. With methane as propellant it was possible to reduce the injection speed keeping a momentum flux ratio $J$ in a realistic range. The decrease of the injection velocity yields less stable flames that are more receptive to external pressure or velocity fluctuations. All tests were carried out with the chamber pressure stabilized at 0.9 MPa. The oxygen injection parameters were kept constant while the methane injection velocity and temperature were changed. Table 1 summarizes the different operating conditions.

### D. Test Procedure

For each operating point, three runs are required to investigate the acoustic response and the flame behavior. The changing parameter between the three runs is the external modulation applied to the system. The first test carried out without external modulation serves as a reference.

In the second run, the modulation frequency is swept linearly, and the excitation frequency is changed continuously from 500 to 3500 Hz at a rate of 150 Hz $s^{-1}$. The rate of change of this linear sweep was selected by taking into account the frequency response of the system or equivalently the damping characteristics of the system as determined from previous experiments.

Using a wave train modulation, it was found that the experimental pressure signal decayed experimentally like $A \exp(-\alpha t) \cos(2\pi f t)$, where $f$ is the modulation frequency, $A$ the amplitude, $t$ the time, and $\alpha$ the damping coefficient. Data fitting provided a value $\alpha = 200\ s^{-1}$. This was used to estimate the resonance bandwidth $\Delta f$ of a second-order system representing the chamber response $\Delta f = \alpha/\pi$. Using this result, it was possible to determine the system bandwidth: $\Delta f \simeq 60$ Hz. This gives the typical spectral width of the combustor resonant modes. The frequency ramp at 150 $Hz \cdot s^{-1}$ is slow enough to obtain a suitable system response.

A short time Fourier transform analysis is used to identify the modal eigenfrequencies. For each of these frequencies, the phase difference between the pressure transducers is calculated in order to determine the modal structure.

The last run is carried out by exciting the system at the first transverse eigenfrequency deduced from the second test. During this procedure, the first and last runs are used to compare the flame structure without and with modulation; the intermediate test provides the acoustic response in the range of frequencies traversed by the linear sweep.

## III. Experimental Domain Exploration

Experimental results, exposed in Sec. IV, define the acoustic response of the system. Three acoustic modes are revealed between 1 and 3 kHz. The frequency of each mode can be accurately determined experimentally, but the modal structures must be deduced from measurements on the lateral walls. It is first important to see if predictions agree with measurements. Calculations are here used to interpret and enhance the limited amount of experimental data and explain acoustic coupling effects between the modulator and the combustor cavity. Injection parameters are then varied to determine ranges of highest sensitivity to external modulation.

### A. Analytical and Numerical Modal Identification

Analytical calculations provide a rough estimate of the resonant frequencies. It is shown however that numerical simulations are required to predict the modal structures and their frequencies in an accurate way and suitably account for the coupling between the modulator and the chamber.

In both cases the mean temperature in the system must be deduced from injection mass flow rates and temperatures. Tests on real engines have shown that these two parameters have a strong influence on the stability domain.[6]

The chamber dimensions have been chosen to place the eigenfrequencies above 1 kHz. An analytical expression for the eigenfrequencies is easily found if the chamber is treated as a closed rectangular cavity without flow neglecting the auxiliary nozzle. The eigenfrequencies are then given by

$$f_c(n_x, n_y, n_z) = \frac{c}{2}\left[\left(\frac{n_x}{l_x}\right)^2 + \left(\frac{n_y}{l_y}\right)^2 + \left(\frac{n_z}{l_z}\right)^2\right]^{\frac{1}{2}}$$

where the speed of sound is calculated through the relation $c = [\gamma(T_{\text{ad}})rT_{\text{ad}}]^{1/2}$.

The adiabatic state is calculated with the CHEMKIN library from initial conditions of pressure and temperature for different values of the mixture ratio $E$. The pressure is fixed at the experimental value of 0.9 MPa. The initial mixing temperature of methane and oxygen is equal to 200 K. Speed-of-sound values deduced from $\gamma$, $T_{\text{ad}}$, and $r$ are 900, 980, and 1175 $\text{ms}^{-1}$ for $E = 0.6$, 0.8, and 1.2, respectively. Rough frequency estimates are obtained for two of the modes. An intermediate mode observed experimentally is not retrieved because the coupling between the secondary nozzle and the main chamber is not included.

This can be improved by numerical calculations taking into account a precise description of the geometry. Numerical simulations yield more accurate eigenfrequencies and the corresponding modal structure. The calculations are based on a finite element method solving the wave equation $\nabla \cdot (c^2 \nabla p') + \omega^2 p' = 0$ together with homogeneous boundary conditions such as a null acoustic pressure or a null acoustic normal velocity. This eigenvalue problem is solved with the MESA-3D code developed at EM2C.[27]

The mesh includes the chamber and the secondary nozzle. The boundaries are treated as rigid walls, which is a reasonable approximation for the two nozzle impedances. The temperature is considered to be uniform and is set to the previously calculated adiabatic value. The calculated frequencies are shown in Fig. 3 for different mixture ratios $E$ and the pressure distribution corresponding to the three first modes are plotted in Fig. 4c.

As observed experimentally, an additional mode is generated between the first longitudinal and transverse modes. Its structure is quite similar to that of the first transverse mode. It involves the side nozzle and the main chamber and features a coupled motion in these two cavities. The frequency of this mode is slightly overestimated compared to the experimental result. The difference is probably caused by the simplified boundary condition at the output of the secondary nozzle. Simulations without the secondary nozzle do not show this mode. The first longitudinal and transverse modes have standard structures. Experimentally, strong interactions have been observed between acoustics and combustion for the intermediate and first transverse modes.

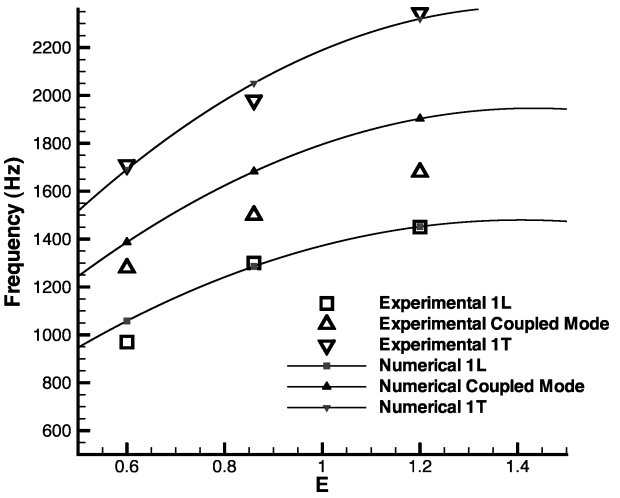


**Fig. 3 Theoretical and experimental eigenfrequencies of the multi-injector test bench vs the mixture ratio ($E = \dot{m}_{\text{LOx}}/\dot{m}_{\text{CH}_4}$).**

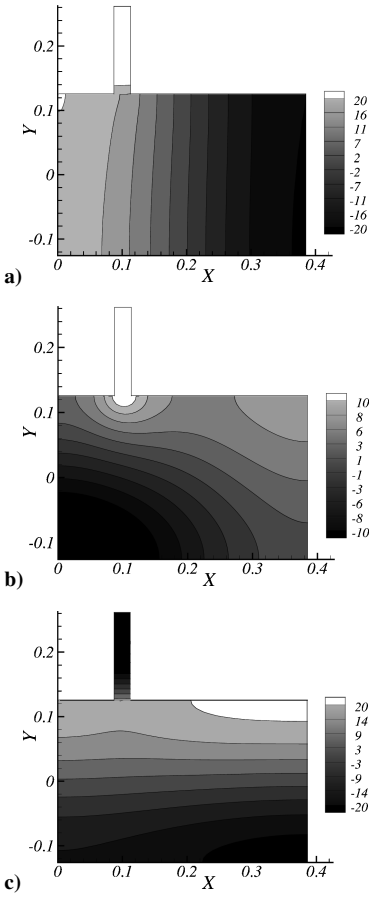


**Fig. 4 Structures of the three first acoustic modes in the combustion chamber calculated numerically: a) first longitudinal at 1452 Hz, b) coupled mode at 1903 Hz, and c) first transverse at 2320 Hz.**

## B. Influence of Injection Parameters

### 1. *Influence of the Methane Injection Flow Rate*

Methane is injected at three different flow rates: 50, 70, and 100 $\text{g} \cdot \text{s}^{-1}$. The corresponding injection velocities are 90, 150, and 200 $\text{m} \cdot \text{s}^{-1}$.

Figures 5a–5c show the average emission of OH* radicals for tests carried out without external modulation at three different methane flow rates. Without modulation, the flame is longer when the methane flow rate is decreased. This is so because at low velocity atomization is less efficient and produces larger droplet sizes, which in turn require more time to vaporize. Burning then takes place on a longer distance.

Figures 5d–5f show the average OH* radical emission when the flames are externally modulated at the eigenfrequency of the first transverse mode for different flow rates. A visible effect of the external perturbation is the expansion of the reactive zone. The flame expansion rate is more important in the case of low injection velocity. When the methane flow rate equals 50 $\text{g} \cdot \text{s}^{-1}$, the mean flame angle is 18 deg, whereas it is only 9 deg for the highest injection speed. At the same time the amplitude of the pressure oscillations is doubled. The change in expansion rate indicates that the system is sensitive to external perturbations. Flames stabilized at low methane injection velocities are clearly more sensitive to the external modulation.

At least three explanations can justify the strong coupling observed at the low methane injection velocity.

1) The hydrodynamic instability frequencies are reduced and come closer to the acoustic frequencies giving rise to a possible coincidence. This can be discussed in terms of a Strouhal number

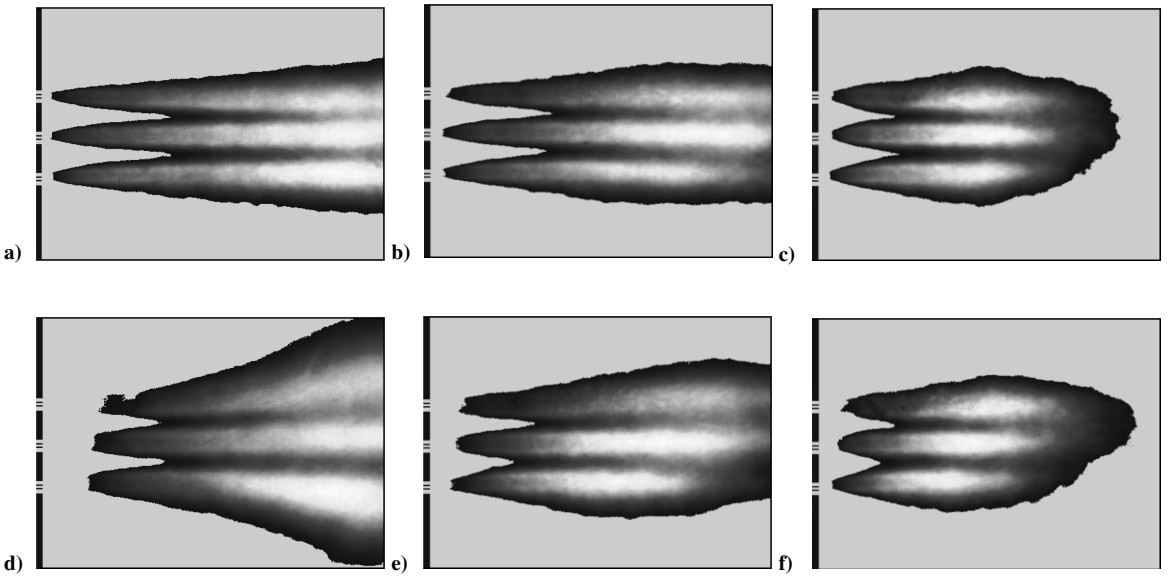


**Fig. 5 Averaged OH* emission for a, b, c) nonmodulated tests, d, e, f) modulated test, and different methane flow rates: a, d) 50 g · s$^{-1}$, b, e) 70 g · s$^{-1}$, and c, f) 100 g · s$^{-1}$.**

defined by $Sr = fd/U$, where $f$ is the hydrodynamic frequency, $d$ the hydraulic diameter of the methane annular injector, and $U$ the injection velocity. If the Strouhal number $Sr$ and the injection diameter $d$ remain constant, when the injection velocity decreases the hydrodynamic frequency decreases by the same order of magnitude.

2) The flame length increases as a result of a slower atomization of the liquid oxygen when the shear rate decreases. The level of pressure fluctuations can be significant enough to improve the atomization process. The external modulation generates transverse velocities that can accelerate the jet breakup. A strong transverse dispersion can be produced compared to the case where atomization is only controlled by the natural shear.

3) The pressure differential in the injector decreases with the injection velocity. This could lead to a coupling of the combustion chamber with the injection lines. Pressure transducers are placed on the manifold, but their positions are relatively far from the injection plane. The corresponding data do not provide reliable indications on the dynamics taking place in the chamber, and it is not possible to conclude at this stage on a possible coupling between the combustion chamber and the injection lines.

The physical parameter leading to the strong interaction between combustion and pressure fluctuation is not precisely determined, but the hot-fire tests already indicate that at low injection velocities the flames are more receptive to external modulation. This occurs for the operating point F50-T280 (Table 1).

### 2. *Influence of the Methane Injection Temperature*

The decrease of the methane injection temperature can also influence the flame response to acoustic perturbations. When methane is injected at low temperature, the liquid oxygen will need a longer time to atomize and vaporize, and its burning might be delayed. The chemical time can also be increased under lower temperature conditions. Tests have been carried out at low velocity and low injection temperature (operating point F50-T180). Methane is still gaseous, but its temperature is 180 K.

Figure 6 presents the instantaneous OH* emission as a function of the methane injection temperature and external modulation. Without modulation (Figs. 6a and 6b), low temperature injection induces an expansion of the emission region. The angle is equal to 9 deg for ambient injection temperature. At low injection temperature, the angle takes a larger value of 15 deg, and the instantaneous distributions are more ragged. A higher variability between successive snapshots is also observed. The reactive zone oscillates showing an unstable behavior of combustion, meaning that the flame is less stable when methane is injected at low temperature. The effect of modulation is visible in the average emission images presented in Fig. 7. When the modulation is on, the expansion rate under low injection temperature changes to a lesser extent when compared to the ambient injection conditions (Figs. 7c and 7d). This expansion modification is also apparent in the instantaneous images (Figs. 6c and 6d). This indicates that the natural flame obtained under low injection temperature is less stable but also less sensitive to external modulations.

The effect of a decrease in methane injection temperature has complex consequences that would require further systematic tests currently not available. In what follows we will only examine experiments carried out with methane injected at ambient temperature. These tests can be used to determine the parameters that yield a stable flame in the absence of excitation and a flame sensitive to external modulations. The injection parameters used for the systematic study correspond to the operating point F50-T280.

## IV. Results

Instantaneous OH* and CH* radical emissions are displayed in Fig. 8 for this operating point. The instantaneous images show spatial distribution of light intensity originating from the flame. The emission of the two radicals OH* and CH* are quite similar and feature the same patterns of interactions between the flame fronts. Well-localized reactive spots can be identified, and large-scale eddies are observed.

The maximum combustion intensity appears in the second part of the combustion chamber, and the flame seems to be lifted. This is caused by the integration of the emission over the line of sight. The projection of the radiated emission on the camera induces an artificial enhancement of the intensity. The intensity scale is then displaced towards the largest values, leading to a lack of information close to the injector. The Abel transform is not feasible in such configurations because they are not symmetric. This point is amplified for the modulated hot-fire test where the reaction rate increases. When examining intensity maps, this should be kept in mind.

Figure 9a shows the pressure signal recorded during a linear frequency sweep (signal provided by sensor C3 in Fig. 1). One finds three resonant peaks. Fast Fourier transforms of the pressure signals (Fig. 9) are used to determine the resonant frequencies. The three peaks are located at 1450, 1680, and 2345 Hz. It is then useful to plot high-pass filtered pressure signals detected on the upper and lower walls to identify the different modes.

The initial resonance corresponds to the first longitudinal mode, and the second defines the coupled mode between the chamber and the secondary nozzle. The third eigenfrequency characterizes the first transverse mode. This latter is deduced from the phase between the five sensors in the combustion chamber plotted in Fig. 10. The

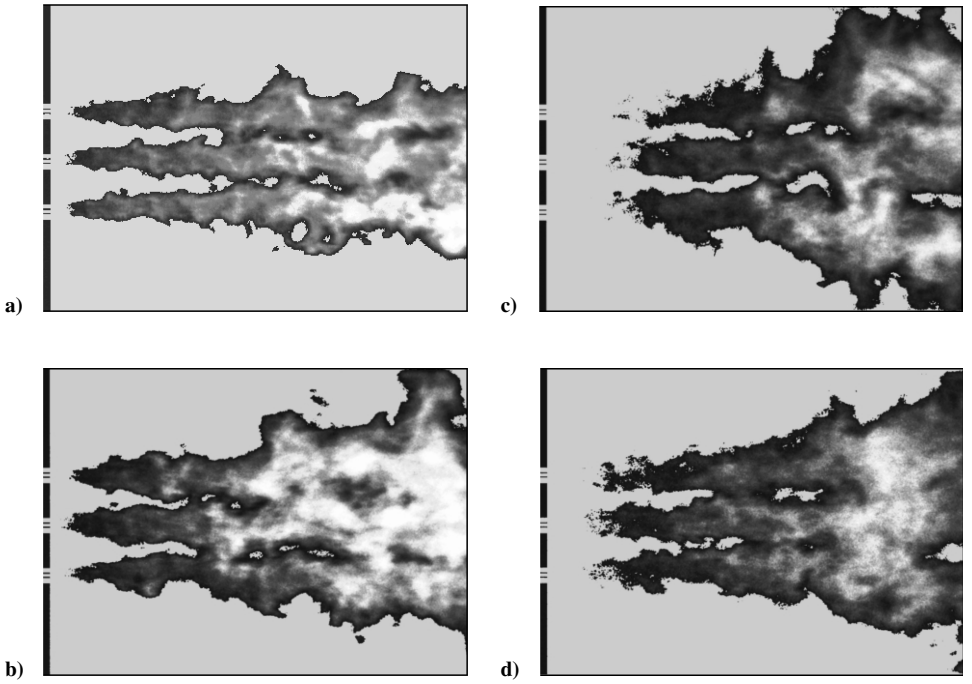


**Fig. 6 Instantaneous OH* emission for a, b) nonmodulated tests, c, d) transversally modulated tests, and different methane injection temperature: a, c) 280 K and b, d) 180 K. The modulation frequency corresponds to the 1T mode.**

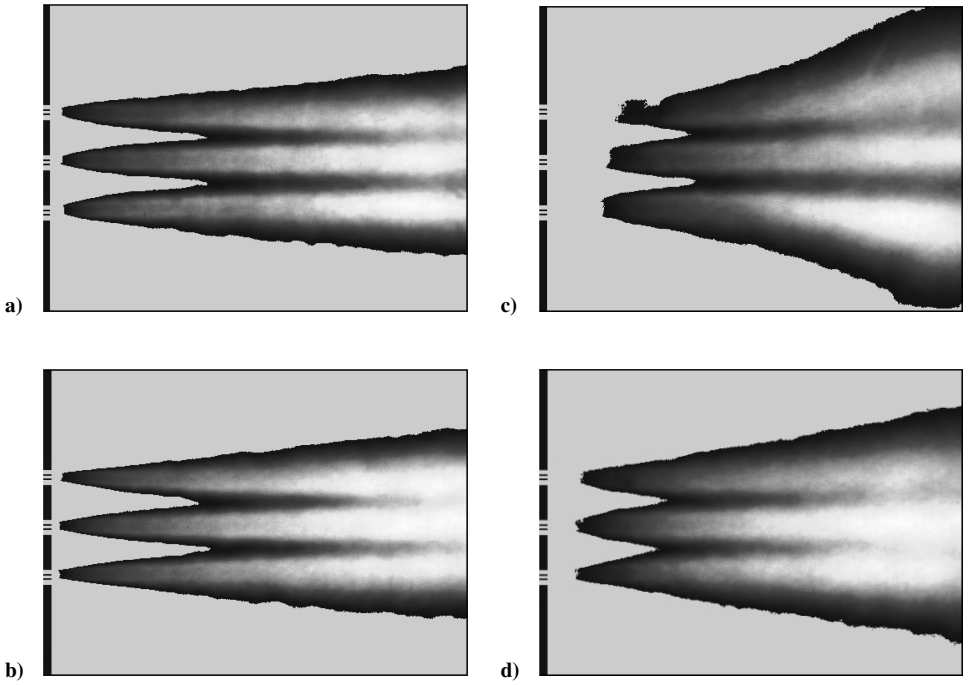


**Fig. 7 Average OH* emission for a, b) nonmodulated tests, c, d) transversally modulated tests, and different methane injection temperature: a, c) 280 K and b, d) 180 K. The modulation frequency corresponds to the 1T mode.**

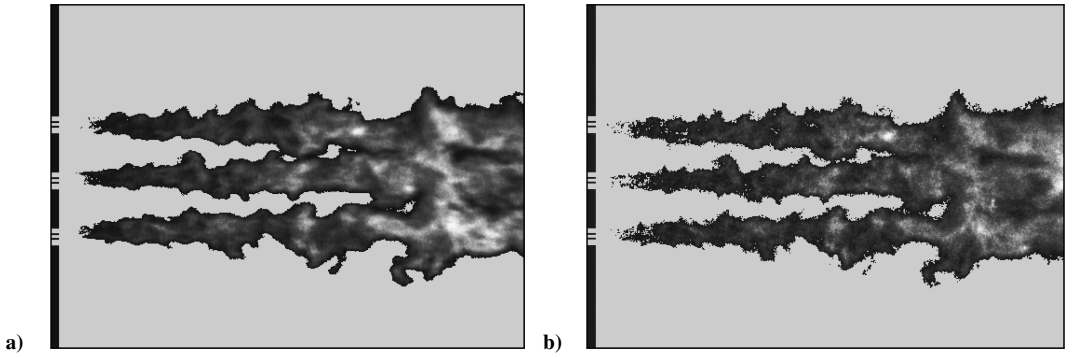


**Fig. 8 Instantaneous (exposure time = 10 $\mu$s) a) OH* and b) CH* emission without external modulation for $E = 0.6$.**

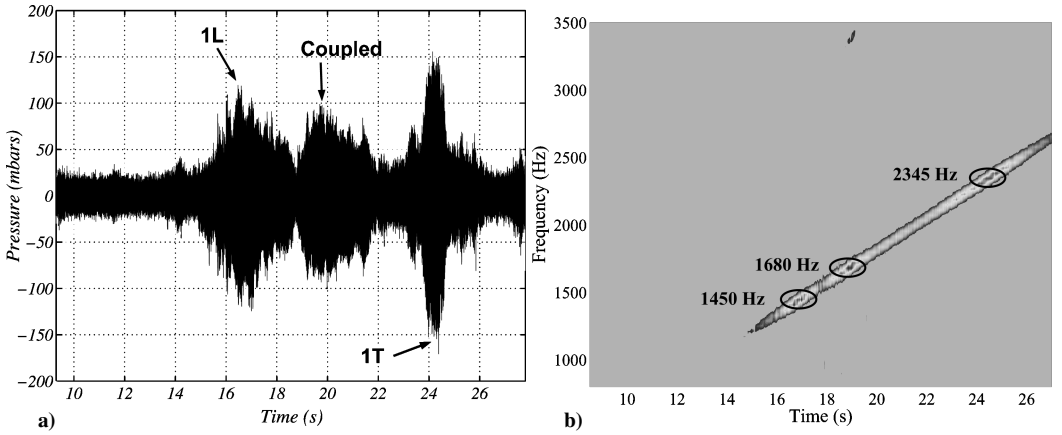


**Fig. 9 Pressure variation during a frequency sweep modulation at a) 100 Hz · s$^{-1}$ and its b) fast Fourier transform.**

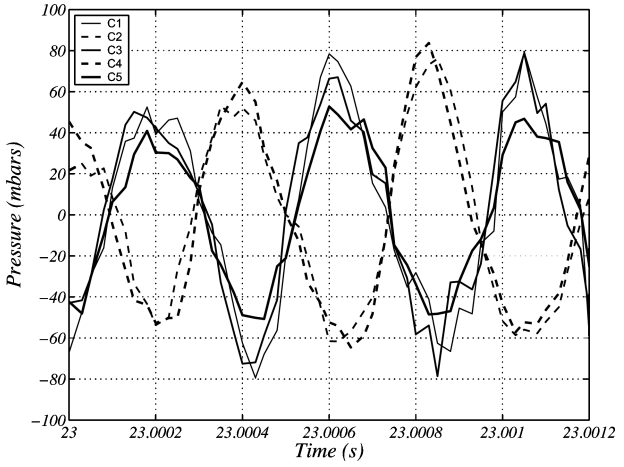


**Fig. 10 Five pressure sensors at the first transverse mode frequency. The three top pressure sensors (odd sensor numbers) are out of phase with the two bottom pressure sensors (even sensor numbers).**

odd-numbered sensors (continuous line) correspond to the three top transducers while the even-numbered sensors (dashed line) are located on the lower wall of the combustion chamber. The top sensors are rigorously out of phase by 180 deg with respect to the bottom units, a situation which corresponds to the first transverse mode shape.

Because the spanwise dimension of the chamber is quite small, the eigenfrequency of the first mode in the third direction is situated well above the frequencies of interest, and only longitudinal and transverse modes can readily appear. Data accumulated over many years of research indicate that high-frequency combustion instabilities are mostly coupled by transverse oscillating modes. It is then logical to modulate the combustion chamber at the eigenfrequency corresponding to the first transverse mode (2345 Hz) and see how the flames respond to this external forcing.

When the chamber is externally modulated at the frequency of the first transverse mode, the pressure transducers confirm the resonance of the system. The pressure signal spectral densities feature a peak at the modulation frequency. In the absence of modulation, the rms pressure reaches 30 mbar. This quantity is equal to 650 mbar when the modulator is operating, which corresponds to 7% of the average chamber pressure. The coupling between acoustic modulation and combustion amplifies the pressure oscillations by a factor 20.

This level modifies the flame dynamics. It was shown in previous studies that the toothed wheel could generate pressure waves of a reasonable amplitude when the system is tuned on a resonant frequency.[20] This is however the first test where the amplitude of oscillations is so high. One of the challenges in this study of high-frequency instabilities in a laboratory-scale experiment is to generate a strong external modulation, and the modulation wheel serves this purpose well. It provides a precise frequency control and a good level of excitation.

The intensified cameras show the interactions between pressure waves and cryogenic flames. Figure 11 presents instantaneous images of OH* emission without (Fig. 11a) and with (Fig. 11b) external modulation. The emission images are plotted on the same intensity scale. They feature fundamental modifications in the flame structures. Without excitation the three flames spread as classical turbulent jet flames, with a small expansion angle. Turbulent structures are convected without significant interactions. The external modulation intensifies the level of fluctuation. The flame expansion angle is augmented, and the size of the convected reactive vortices increases. The transverse velocity generates larger structures that lead to flame interactions and collision of adjacent shear regions.

The image presented in Fig. 11b corresponds to the middle of the modulation period, when the pressure field is uniform in the chamber. A direct correlation between the pressure phase and the position of the flames was expected but not obtained. This is probably because the fluctuation levels associated with acoustic (coherent) modulations are important but still not high enough compared to turbulent (random) fluctuations. However high-speed films clearly show the transverse motion of the flow under acoustic modulation.

The average light emission level (roughly corresponding to the reaction rate) is also increased with the modulation. The large reactive structures induced by the external modulation improve the mixing process and presumably the liquid jet atomization. This has direct consequences on combustion intensity. A thermocouple located in the lower chamber wall (not in direct contact with the hot gases) features a large increase of the wall temperature when the system is modulated at the frequency of the first transverse mode.

The injection plane of the combustion chamber has dimensions significantly greater than the injector. The fresh propellants are injected in the middle of the chamber, far from the top and bottom walls. This geometry differs from that of real engines where the injection plane features closely packed injection units. This induces at least three distortions with respect to liquid rocket engine configurations: 1) a recirculation region of fresh methane can develop in the upper and lower sides of the chamber above and below the injector group, 2) effects of heat losses at the walls are minimized, and 3) interaction between the transverse mode and the flames takes place over a limited region. This affects the flame expansion rate, which is a visible effect of the coupling between acoustic wave and combustion. The change in spreading rate might not be as strong in real engines. However, the comparison between the two tests (modulation free and modulated) gives relevant information on the flame motion and on the interaction process.

The dynamic behavior of heat release is also detected by the PM. These sensors are vertically aligned and measure the oscillating OH* light emission from the reactive regions. Figure 12 presents the spectral analysis of the bottom PM signals for modulated and nonmodulated tests. The average shape of the power spectral density features a strong low-frequency component detected around

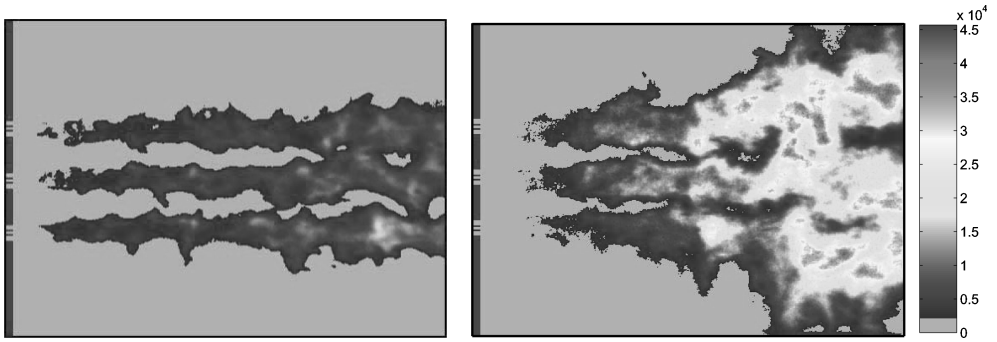


**Fig. 11 Instantaneous OH* emission (exposure time is 2 $\mu$s) a) without modulation and b) with modulation at 2345 Hz represented with the same intensity scale (arbitrary units).**

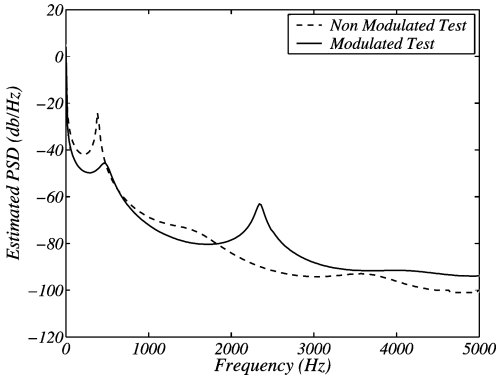


**Fig. 12 Fougere spectral analysis of the bottom photomultiplier for nonmodulated (one peak at 360 Hz) and modulated (two peaks at 450 and 2350 Hz) hot-fire tests.**

400 Hz (exactly 360 Hz for the nonmodulated test and 450 Hz for the modulated test). This frequency corresponds to the natural turbulent combustion process. The spectral density also features a peak at the modulation frequency indicating that light intensity oscillation occurs at the excitation frequency. The pressure fluctuations generated by the rotating wheel have a direct influence on the light emission and then on the heat-release rate.

The pressure transducers and the photomultipliers locations are shown in Fig. 1. The odd-numbered sensors and photomultiplier are in the top part of the chamber while the even-numbered probes are located in the bottom part. Using these elements, it is possible to examine the phase difference between the signals collected from the two parts of the chamber. As shown in Fig. 10, the top pressure transducers are out of phase by 180 deg with respect to the bottom ones at the modulation frequency (2345 Hz) indicating the presence of the first transverse eigenmode. This mode can also be observed by analyzing the photomultiplier signals.

Similarly, the phase of the photomultipliers is 180 deg at the forcing frequency. The cross-spectral density diagram shows that the low-frequency perturbations are uncorrelated and natural combustion fluctuations of the top and bottom parts are not linked. In contrast, at the modulation frequency, the coherence of the two PM is close to 1, and light emission in the combustion chamber oscillates between top and bottom parts of the chamber. The two signal amplitudes are nearly equal.

It is also important to examine the phase difference between the fluctuating heat-release $q'$ and the pressure fluctuations $p'$. These two quantities oscillate at the modulation frequency, and their magnitude squared coherence, displayed in Figs. 13a and 13b, is high enough ($\simeq$0.7) to prove that heat release and the pressure fluctuations are strongly correlated. The phase difference between the two PMs and the pressure sensors has been calculated for all of the possible combinations. Figure 13c gathers the reduced phases between the two PMs and the five pressure transducers at the modulation frequency (2345 Hz). The sensor numbers are placed below the horizontal axis and the corresponding value of the reduced phase

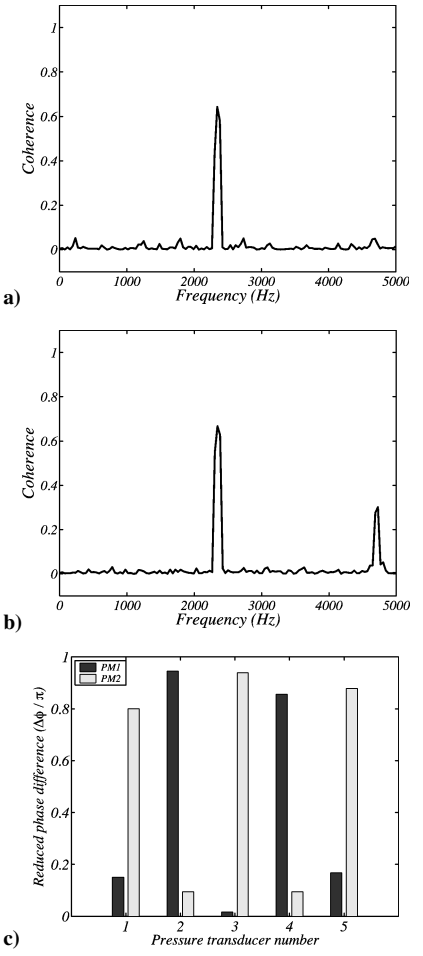


**Fig. 13 Magnitude squared coherence ($|S_{xy}|^2/S_{xx}S_{yy}$) a) between PM 1 and C5 then b) between PM 2 and C5, and c) reduced phase difference between the two PM and the five pressure transducers at the modulation frequency (2345 Hz).**

differences between each sensor, and the two PMs are plotted as bars in this diagram. PM1 is in phase with pressure transducers C1, C3, and C5, while PM2 is out of phase with these same sensors. In contrast, PM2 is in phase with C2 and C4 while PM1 is out of phase with them. In other words, the PMs and the pressure transducers are not only strongly correlated, but the top and bottom PMs are respectively in phase with the top and bottom sensors.

This indicates that the fundamental mechanism leading to combustion instabilities, which involves a strong and coherent coupling between the heat-release and pressure fluctuations, is operating and that the flames are directly sensitive to the excitation frequency. However, low-frequency perturbations still dominate the motion

in the high-speed film images. The camera sampling rate is set to 20,000 frames per second with a window of $256 \times 128$ pixels. The flame motion is observed at the end of the chamber, where the flames interact. The high-speed film features the oscillating transverse motion of the flames at 2345 Hz, but lower frequencies corresponding to convection of reactive vortices are quite visible, indicating that the high-frequency excitation enhances to a great extent low frequency (~400 Hz) vortices. The coupling between the high-frequency transverse oscillating motion and the low-frequency longitudinal convection appears to be an important feature of the phenomenon.

## V. Discussion

The data reported in the preceding section can now be used to discuss the following aspects: 1) coupling observed at the modulation frequency between the photomultipliers and the different pressure transducers, 2) similarities and differences between the present externally induced oscillations and self-sustained high frequency instabilities, and 3) link between the imposed high-frequency modulation and the low-frequency turbulent fluctuations. These three points are considered successively. High-frequency combustion oscillations are induced in the present experiments by imposing a large-amplitude transverse mode with a pressure fluctuation of the order of 8% of the mean pressure. A coupling between combustion and the first transverse mode is indeed obtained and leads to enhanced acoustic fluctuations.

The data indicate that heat-release fluctuations take a spatial structure which resembles that of the transverse mode and oscillates in phase with the pressure. This could lead to self-sustained oscillations but does not happen here because the losses exceed the gain associated with this coupling.

Consequently, the flame response differs from what is observed from earlier experiments. This can be seen by examining some of the early experiments on self-sustained high-frequency instability. One can use for example model-scale investigations providing high-speed records like those of Tischler and Male[8] or Barrère and Corbeau[28] to compare the present data with earlier observations. In Ref. 8 a 10-cm-diam, 1-m-long model-scale rocket engine is equipped with a slit extending over part of the circumference of the system. A video camera records the light intensity through the transverse slit located at 14 cm from the injection plane. Figure 14 shows the light observed when a 6000-Hz azimuthal mode is set up in the chamber. A luminous zone moves across the chamber in a helical way, and this is recorded by the camera as a periodic energy release in the upper and lower sides of the chamber. The frequency of positive excursions of heat release in the upper and lower parts of the chamber coincides with the oscillation frequency. It is then natural to infer that positive heat-release fluctuations occur at the same frequency as the transverse velocity fluctuations.

Similar phenomena have been identified on the present experiments. The light emission, recorded by the photomultipliers, features the same frequency as the first transverse mode, indicating that the periodic heat release is coupled to this mode. The most intense reaction-rate position in the chamber also oscillates between the top and bottom sides of the combustion chamber. From the high-speed camera it is possible to create numerically a virtual slit similar to the real aperture used in Ref. 8. In each frame, a one-pixel column is extracted and placed next to the same column from the previous frame. The temporal evolution of light intensity in a given cross section can be retrieved in this way.

Figure 15 presents these type of data for natural and modulated hot-fire tests. The oscillations of the modulation-free combustor appear clearly around 400 Hz. When modulated, the combustion zone is enlarged and more intense, but no regular pattern can be

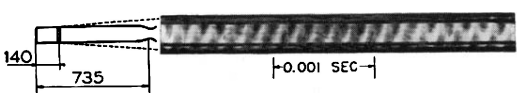


**Fig. 14 Streak photograph of rotary screaming waves in a cross section at 14 cm from the injection plane (from Tischler and Male[8]).**

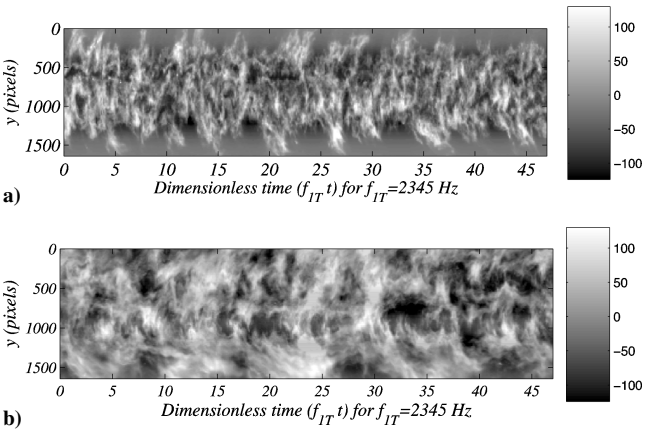


**Fig. 15 Temporal evolution of the flame light emission in a cross section at 12 cm from the injection plane for a) nonmodulated and b) modulated test. The average flame emission is subtracted from the instantaneous values.**

observed at the modulation frequency. This is so because two competing phenomena generate perturbations in the flowfield. The first is shear flow turbulence, and the second is the fluctuating acoustic field. An order-of-magnitude analysis indicates that the displacement induced by the acoustic field is largely inferior to that related to turbulence. The average pressure fluctuations generated by the rotating wheel are $p' \simeq 700$ mbars providing velocity fluctuation $v' \simeq p'/\rho_0 c \simeq 37\ \mathrm{m \cdot s^{-1}}$ considering $c = 1000\ \mathrm{m \cdot s^{-1}}$ and $\rho_0 = 1.87\ \mathrm{kg \cdot m^{-3}}$; this yields a maximum displacement of 1.5 cm during each period of modulation. This transverse displacement is observable in the high-speed film, but it remains small compared to the chamber dimensions. The transverse oscillations are still too small to be observed independently from the low-frequency motion around 400 Hz.

A different view of this issue can be obtained by comparing the induced transverse velocity $v'$ with typical turbulent fluctuations $v'_t$ existing in the present configurations. The turbulence level in the jet flames is typically of about 15% of the mean injection velocity difference between the methane and oxygen streams.[29,30] This gives rise to turbulent fluctuations of the order of $15\ \mathrm{m \cdot s^{-1}}$ in the F50-T280 test case, and the ratio $v'/v'_t$ is of about 2. It appears that this value is already sufficient to modify the flame dynamics but is too low to have the flow switch from an essentially turbulence controlled organization to a high-frequency nearly periodic motion.

Having established that the situation at hand is intermediate in the sense that it is controlled by competing phenomena (high-frequency oscillation, low-frequency fluctuations), one can now discuss the coupling observed in such circumstances. Indeed, one unusual feature is that the high-frequency modulation also enhances the low-frequency motion. The flow is dominated by natural instabilities, but the transverse perturbations improve the rate of entrainment of reactive material in the larger-scale vortex patterns.

The instantaneous OH* emission images show that the combustion intensity is modified, that the spatial distribution is changed, and that sizes of the turbulent burning structures are augmented. The flame expansion and the emission amplitude increase drastically under external modulation. Reaction spreads over a wider region in the chamber, which corresponds to an improved and more homogeneous atomization than without modulation. The eddy sizes are also increased by the external modulation. The reactive spots observed with the intensified charge coupled device cameras are larger and their convection in the downstream direction is more easy to detect.

An examination of the time evolution of burning spots also indicates that the local reactive layers are submitted to an augmented strain rate, which in turn increases the local reaction rates.

## VI. Conclusions

The dynamics of a multiple-injector combustor is investigated under high-frequency transverse excitation. The study is carried out

on a rectangular cross-section system featuring three coaxial injectors fed with cryogenic propellants. A modulation system is used for external excitation. The system eigenmodes are first identified by performing a linear frequency sweep. Injection parameters are varied to determine conditions under which combustion becomes sensitive to external oscillations. Such conditions are observed when the methane stream velocity is relatively low. Pressure sensors provide the acoustic response of the system to the external modulation and clearly indicate that the spatial distribution is that expected for the 1T mode. The eigenfrequencies of the combustion chamber are determined numerically and identified experimentally.

When modulated at the first transverse frequency, the pressure amplitude oscillation reaches 7% of the average chamber pressure, which is significant enough to induce a strong coupling between acoustics and combustion. This coupling manifests itself as a visible enhancement of flame spread, and radiation from the flame is augmented by a large factor while thermocouples placed on the lateral walls detect a rapid increase in temperature. The OH* emission intensity, which can be linked to the heat-release rate, increases significantly. Photomultipliers indicate that the most intense emission area in the chamber oscillates transversally at the modulation frequency. A phase analysis carried out at that frequency indicates that the pressure and OH* emission have similar spatial distributions and oscillate in phase. This behavior has also been observed with the high-speed camera, which also features enhanced reactive vortices convected in the downstream direction at a lower frequency.

## Acknowledgments

This study was supported by Snecma, Centre National d'Etudes Spatiales and Centre National de la Recherche Scientifique in the framework of the French–German program on High Frequency Combustion Instability. Experiments were carried out on the Mascotte test bench with the assistance of the liquid-rocket-propulsion team of ONERA.

## References

[1]Candel, S., "Combustion Dynamics and Control: Progress and Challenges," *Proceedings of the Combustion Institute*, Vol. 29, No. 1, 2002, pp. 1–28.

[2]Mongia, H. C., Held, J., Hsiao, G. C., and Pandalai, R. P., "Challenges and Progress in Controlling Dynamics in Gas Turbine Combustors," *Journal of Propulsion and Power*, Vol. 19, No. 5, 2003, pp. 822–829.

[3]Lee, J. G., and Santavicca, D. A., "Experimental Diagnostics for the Study of Combustion Instabilities in Lean Premixed Combustors," *Journal of Propulsion and Power*, Vol. 19, No. 5, 2003, pp. 735–750.

[4]Lefebvre, A., *Gas Turbine Combustion*, Taylor and Francis, Philadelphia, 1999.

[5]Culick, F. E., and Yang, V., "Overview of Combustion Instabilities in Liquid-Propellant Rocket Engines," *Liquid Rocket Engine Combustion Instability*, edited by V. Yang and W. Anderson, Vol. 169, AIAA, Washington, DC, 1995, pp. 3–37.

[6]Hulka, J., and Hutt, J., "Instability Phenomena in Liquid Oxygen/Hydrogen Propellant Rocket Engines," *Liquid Rocket Engine Combustion Instability*, Vol. 169, AIAA, Washington, DC, 1995, pp. 39–71.

[7]Harrje, D., and Reardon, F., "Liquid Propellant Rocket Combustion Instability," NASA SP-194, Washington, DC, 1972.

[8]Tischler, A. O., and Male, T., "Oscillatory Combustion in Rocket-Propulsion Engines," *Gas Dynamics Symposium*, 1956, pp. 71–81.

[9]Rogers, D. E., and Marble, F. E., "A Mechanism for High-Frequency Oscillation in Ramjet Combustors and Afterburners," *Jet Propulsion*, June 1956, pp. 456–462.

[10]Lawhead, R., and Combs, L., "Modeling Techniques for Liquid Propellant Rocket Combustion Processes," *Proceedings of the Combustion Institute*, Vol. 9, No. 1, 1963, pp. 973–981.

[11]Oschwald, M., Smith, J. J., Branam, R., Hussong, J., Schik, A., Chehroudi, B., and Talley, D., "Injection of Fluids into Superficial Environments," *Combustion Science and Technology*, Vol. 178, No. 1-3, 2006, pp. 49–100.

[12]Anderson, W. E., Miller, K. L., Ryan, H. M., Pal, S., Santoro, R. J., and Dressler, J. L., "Effects of Periodic Atomization on Combustion Instability in Liquid-Fueled Propulsion Systems," *Journal of Propulsion and Power*, Vol. 14, No. 5, 1998, pp. 818–825.

[13]Bazarov, V., and Yang, V., "Liquid Propellant Rocket Injector Dynamics," *Journal of Propulsion and Power*, Vol. 14, No. 5, 1998, pp. 797–806.

[14]Merkle, C. L., Sankaran, V., and Ellis, M., "Computational Simulation of Acoustic Modes in Rocket Combustors," JANNAF 2004-0031, May 2004.

[15]You, D., and Yang, V., "Linear Stability of Baffled Combustion Chamber with Radial and Circumferential Blades," AIAA Paper 2005-930, Jan. 2005.

[16]Tamura, H., Sakamoto, H., Sasaki, M., Takahashi, M., Tomita, T., and Mayer, W., "An Experimental Study on the Stability Characteristics of the LOx/Methane Rocket Combustor," AIAA Paper 95-2359, July 1995.

[17]Mayer, W., and Tamura, H., "Propellant Injection in a Liquid Oxygen/Gaseous Hydrogen Rocket Engine," *Journal of Propulsion and Power*, Vol. 12, No. 6, 1996, pp. 1137–1147.

[18]Fisher, S., Dodd, F., and Jensen, R., "Scaling Techniques for Liquid Rocket Combustion," *Liquid Rocket Engine Combustion Instability*, edited by V. Yang and W. Anderson, Vol. 169, AIAA, Washington, DC, 1995, pp. 545–564.

[19]Vingert, L., Gicquel, P., Lourme, D., and Mènoret, L., "Coaxial Injector Atomization," *Liquid Rocket Engine Combustion Instability*, Vol. 169. AIAA, Washington, DC, 1995, pp. 145–190.

[20]Rey, C., Ducruix, S., Richecoeur, F., Scouflaire, P., Vingert, L., and Candel, S., "High Frequency Combustion Instabilities Associated with Collective Interactions in Liquid Propulsion," AIAA Paper 2004-3518, July 2004.

[21]Rubinsky, V. R., "Combustion Instability in the RD-0110 Engine," *Liquid Rocket Engine Combustion Instability*, edited by V. Yang and W. Anderson, Vol. 169, AIAA, Washington, DC, 1995, pp. 89–112.

[22]Yang, V., Wicker, J., and Yoon, M., "Acoustic Waves in Combustion Chambers," *Liquid Rocket Engine Combustion Instability*, edited by V. Yang and W. Anderson, Vol. 169, AIAA, Washington, DC, 1995, pp. 357–376.

[23]Juniper, M., Tripathi, A., Scouflaire, P., Rolon, J., and Candel, S., "The Structure of Cryogenic Flames at Elevated Pressures," *Proceedings of the Combustion Institute*, Vol. 28, No. 1, 2000, pp. 1103–1109.

[24]Schuller, T., Durox, D., and Candel, S., "Dynamics of Flame and Noise Radiated by a Perturbed Impinging Premixed Jet Flame," *Combustion and Flame*, Vol. 128, Jan. 2002, pp. 88–110.

[25]Schuller, T., Durox, D., and Candel, S., "Self-Induced Combustion Oscillations of Laminar Premixed Flames Stabilized on Annular Burner," *Combustion and Flame*, Vol. 135, Dec. 2003, pp. 525–537.

[26]Crocco, L., and Cheng, S., "Theory of Combustion Instability in Liquid Propellant Rocket Motors," 8 in AGARD Monograph, Pergamon, London, 1956.

[27]Nottin, C., "Développement de Methodes de Prévision des Instabilities de Combustion dans les Foyers Prmelanges," Ph.D. Dissertation, Dept. of Energy, Ecole Centrale, Paris, Dec. 2002.

[28]Barrère, M., and Corbeau, J., "Les Instabilites de Combustion dans les Fusees a Propergol liquide," *Combustion and Propulsion—Fifth AGARD Colloquium*, Pergamon, London, 1962, pp. 637–692.

[29]Hussein, H. J., Capp, S. P., and George, W. K., "Velocity Measurements in a High-Reynolds-Number, Momentum-Conserving, Axisymmetric, Turbulent Jet," *Journal of Fluid Mechanics*, Vol. 258, 1994, pp. 31–75.

[30]Wygnanski, I., and Fiedler, H., "Some Measurements in the Self-Preserving Jet," *Journal of Fluid Mechanics*, Vol. 38, 1969, pp. 577–612.